Atmospheric Research 328 (2026) 108405

Contents lists available at ScienceDirect

Atmospheric Research

journal homepage: www.elsevier.com/locate/atmosres

Microphysical analysis on the impacts of reduced aerosol concentrations on tropical cyclone precipitation in South China Area

Ho Yi Lydia Mak [a,*], Yi Zhang [b], Xiaoming Shi [a]

[a] Division of Environment and Sustainability, Hong Kong University of Science and Technology, Hong Kong, China
[b] Department of Geography and Planning, University of Toronto, Toronto, Canada

ARTICLE INFO

Keywords:
Tropical cyclones
Precipitation
Aerosols
Moist available potential energy

ABSTRACT

Previous studies have discovered that an increase in aerosol concentration could affect the development of precipitation and tropical cyclones. However, with increasing efforts to mitigate climate change, the amount of anthropogenic aerosols in the atmosphere is expected to decrease in the future. This study aims at understanding how such a reduction in aerosol number concentration could affect the precipitation pattern of tropical cyclones through case studies of Typhoon Haikui and Koinu. The Thompson aerosol-aware microphysics scheme in the Weather Research and Forecast (WRF) model is used, and the water-friendly aerosol number concentration is reduced by a factor of 100. For both tropical cyclones, a reduction in aerosol results in consistent expansion of precipitation area due to the enhanced warm rain process. However, the total precipitation of Koinu decreases while that of Haikui increases, depending on whether warm-rain or ice-phase processes dominate and whether upper-level convection is altered.

1. Introduction

Tropical cyclones are great threats to the South China area from May to November each year. In Hong Kong, an average of six tropical cyclones necessitate the issuance of tropical cyclone warning signals annually (Hong Kong Observatory, 2024). These natural hazards bring strong wind, rainfall, and storm surge to the city, with rainfall being the most significant factor for economic losses in the region (Sajjad and Chan, 2020).

Aerosols play an important role in the generation of precipitation through direct radiative effect as well as indirect microphysical effects. Several studies have investigated how natural aerosol sources affect tropical cyclones: Zhang et al. (2009) demonstrated Saharan dust's impact on tropical cyclone eyewall structure, Liu et al. (2022) revealed volcanic aerosols' role in cyclogenesis, and Jiang et al. (2019) quantified sea-salt aerosols' effects through their distinctive large particle size and strong hygroscopicity. In South China, however, anthropogenic sulfate and ammonium aerosols dominate the atmospheric particulate composition (Huang et al., 2014). These hygroscopic aerosols can serve as cloud condensation nuclei, thereby initiating cloud droplet formation. As demonstrated by Yang et al. (2018), aerosol-cloud-precipitation interactions represent the primary mechanism through which aerosols modulate tropical cyclones in this region - a phenomenon that has been widely investigated in previous studies.

Over the years, there has been numerous observational evidence showing that cloud droplet size is smaller and their size distribution is narrower in high-aerosol environments (e.g., Andreae et al. (2004); Yuan et al. (2008)). These lead to less effective collisions between cloud drops, suppressing warm-rain formation (Tao et al., 2012). Rosenfeld et al. (2008) suggest that due to delayed precipitation formation, more water could be brought above supercooled levels and freeze into ice particles, releasing latent heat in the process. Meanwhile, heat is reabsorbed at lower levels when the falling ice melts. These create greater upward heat transport which results in the invigoration of convective clouds, leading to higher rainfall than clean conditions. Such hypothesis is supported by cloud-resolving modeling studies (Khain et al., 2005; Van Den Heever and Cotton, 2007), as well as satellite observations that show a positive correlation between aerosol optical depth and convective cloud properties including cloud fraction and cloud top height (Koren et al., 2005, 2010). However, this so-called cold-phase invigoration mechanism has been questioned since it is based on the unrealistic assumption that condensates in updrafts freeze and unload instantaneously (Varble et al., 2023). Grabowski and Morrison (2020) pointed out that the buoyancy created by additional freezing balances the weight

* Corresponding author.
E-mail address: hylmak@connect.ust.hk (H.Y.L. Mak).

https://doi.org/10.1016/j.atmosres.2025.108405
Received 19 April 2025; Received in revised form 24 June 2025; Accepted 3 August 2025
Available online 7 August 2025

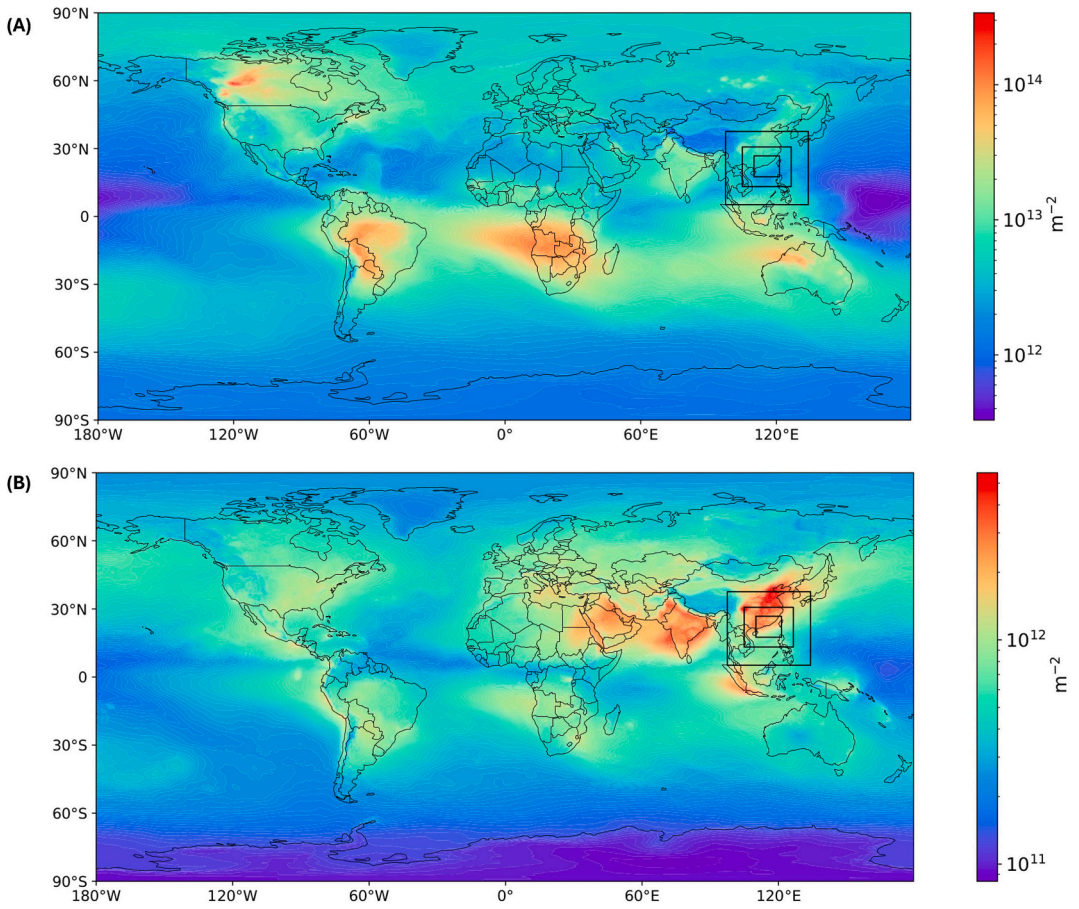

Fig. 1. Average column number density of (A) organic carbon and (B) sulfates in September to October 2023. Hourly column mass density of the two species were obtained from MERRA-2 (Global Modeling and Assimilation Office (GMAO), 2015), and the column number density was calculated by assuming that the aerosol sizes follow a lognormal distribution and using the effective radii and geometric standard deviations from Chin et al. (2002). The black boxes mark the three domains of our simulations.

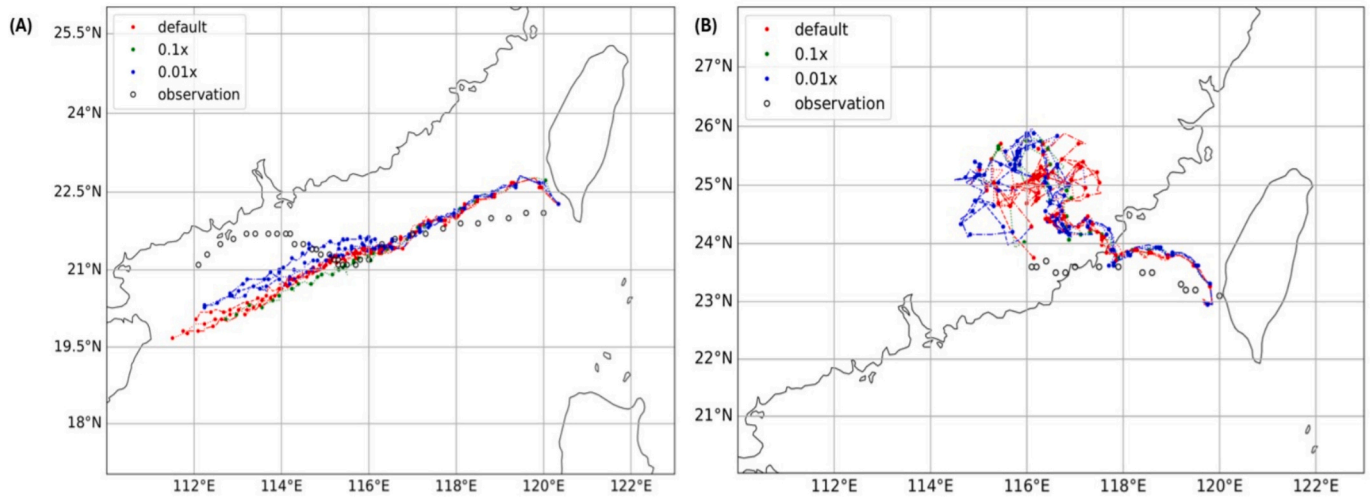

Fig. 2. Tracks of (A) Koinu and (B) Haikui from our experiments (default in red, 0.1× in green, 0.01× in blue) as determined by minimum sea level pressure and observed track (black circles) as given by Hong Kong Observatory (Hong Kong Observatory, 2024a, 2024b). The observed track for Haikui is plotted up to 12 UTC on 5 September 2023, after which the typhoon dissipates. (For interpretation of the references to colour in this figure legend, the reader is referred to the web version of this article.)

of the extra condensate, resulting in no convective invigoration above the freezing level. However, Fan and Khain (2021) argue that the different locations and time scales of droplet ascending and freezing, as well as the additional buoyancy due to additional condensation, deposition and riming, could render cold-phase invigoration possible.

Apart from cold-phase invigoration which is still debated, other

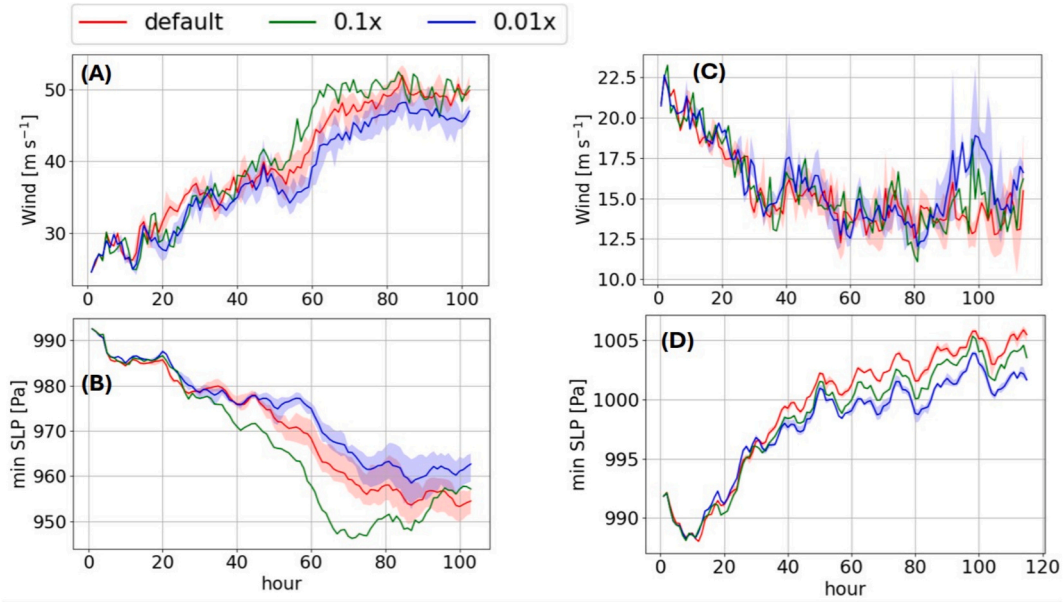

Fig. 3. Maximum surface wind speed and minimum sea level pressure (SLP) of Koinu (A-B) and Haikui (C-D). Default experiment is in red, 0.1× is in green and 0.01× is in blue. Shaded regions mark the range of the results from the ensemble of three simulations. (For interpretation of the references to colour in this figure legend, the reader is referred to the web version of this article.)

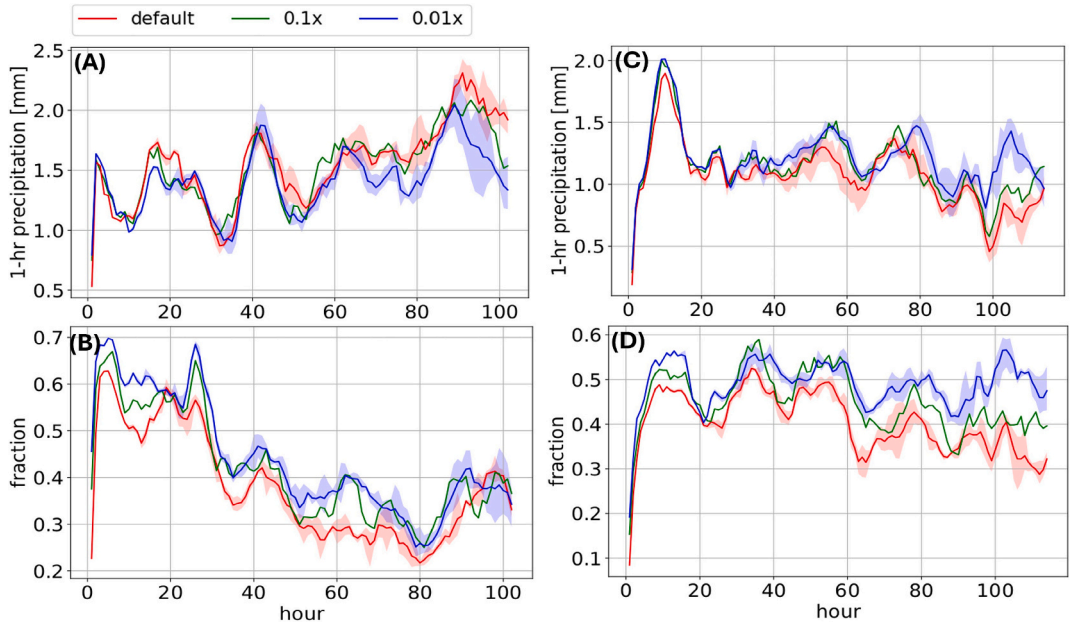

Fig. 4. Mean precipitation and fraction of area with precipitation exceeding 0.01 mm h^{-1} in 600 × 600 km region around low-pressure center of Koinu (A-B) and 800 × 800 km region around low-pressure center of Haikui (C-D). Default experiment is in red, 0.1× is in green and 0.01× is in blue. Shaded regions mark the range of the results from the ensemble of three simulations. (For interpretation of the references to colour in this figure legend, the reader is referred to the web version of this article.)

mechanisms causing the difference in convection in clean and polluted environments are suggested in the literature. The studies by Fan et al. (2018) and Grabowski and Morrison (2020) suggest that invigoration exists below the freezing level, though the authors have not reached a consensus on the mechanism behind. While the former believe that the greater latent heating in polluted environments is due to enhanced condensation rate with increased droplet concentration, the latter believe that it is due to reduced supersaturations increasing buoyancy, which causes stronger updrafts that enhances condensation rates. On the other hand, Tao et al. (2012) suggest that smaller droplets in more polluted conditions could result in stronger evaporative cooling, enhancing the strength of the near-surface cold pool, which could also produce more vigorous convection and thus enhanced precipitation.

Tropical cyclones are mesoscale convective systems that are also affected by aerosol concentration. While several studies have shown that the track of tropical cyclones is hardly affected by aerosol concentration (Cotton et al., 2012; Hazra et al., 2013; Jiang et al., 2016; Pan et al., 2020), it is evident that the intensity of the tropical cyclone could be affected. Hazra et al. (2013) and Jiang et al. (2016) found that precipitation is reduced in polluted environments due to reduced collision and

Table 1
Comparison of average precipitation rates over entire simulation excluding first 24 h in 600 × 600 km region around low-pressure center of Koinu and 800 × 800 km region around low-pressure center of Haikui in mm h^{-1}. "0.1×" and "0.01×" refers to aerosol concentration reduced by a factor of 10 and 100 compared to the default value.

	Koinu			Haikui		
Default		0.1×	0.01×	Default	0.1×	0.01×
Mean precipitation rate (mm h^{-1})						
Entire region	1.55 ± 0.02	1.54	1.42 ± 0.01	1.07 ± 0.05	1.14	1.22 ± 0.07
Region exceeding 0.01 mm h^{-1}	4.07 ± 0.03	3.69	3.21 ± 0.02	2.66 ± 0.09	2.58	2.50 ± 0.02

coalescence. Cotton et al. (2012) found a similar phenomenon when aerosols are first ingested in a simulation of West Pacific Typhoon Nuri, but subsequently, an increased amount of droplets were thrust into higher levels where they freeze and release greater latent heat, thereby intensifying convection and producing more rainfall. Rosenfeld et al. (2012) further suggested that as the convection in peripheral clouds becomes more vigorous, more ascending air is drawn at the periphery of the storm, the low-level airflow towards the eyewall is reduced, weakening the convergence towards the cyclone center. Consequently, the wind speed at the eyewall would reduce. In addition, Jiang et al. (2016) noted that precipitation is increased at the periphery but decreased in the eyewall region when aerosol concentration is high. On the contrary, Herbener et al. (2014) found a strengthening of storm intensity with increasing aerosol concentration. The authors suggested that convective invigoration in the eyewall region and in the outer rainbands could affect storm intensity in opposite ways, resulting in non-linear responses in storm intensity.

Most existing studies put their focus on how increased aerosol concentrations might impact the properties of tropical cyclones. However, with increased emission reduction policies to mitigate climate change, it can be expected that the aerosol concentration in the atmosphere will decline in the future. For the strong mitigation scenarios SSP1 defined in the Sixth Assessment Report of the Intergovernmental Panel on Climate Change (IPCC AR6), global emissions of sulfur dioxide and organic carbon are projected to decrease by around 90 % and 60 % respectively (Chen et al., 2021). A decrease in aerosol concentration is likely to affect microphysics and alter the development of convective precipitation and tropical cyclones. However, it is found that the relationship between aerosol concentration and precipitation patterns is non-linear in convective clouds and tropical cyclones (Wang et al., 2023; Hazra et al., 2013; Jiang et al., 2016), so one cannot extrapolate the trend found in existing studies to predict the changes in a cleaner scenario. Therefore, it

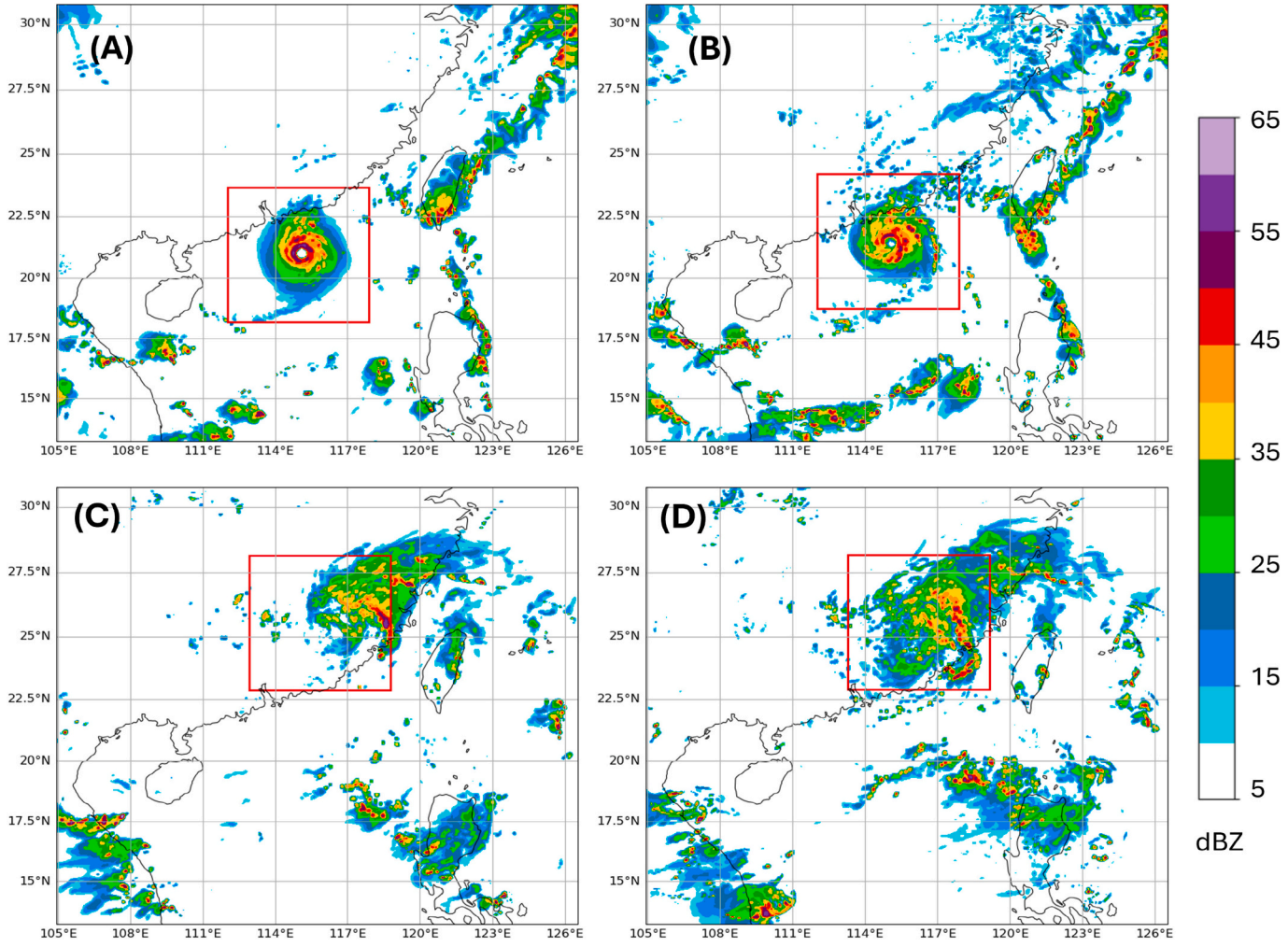

Fig. 5. Composite radar reflectivity of (A) Koinu default and (B) Koinu 0.01× (aerosol concentration reduced by a factor of 100) at 22:00 UTC on 7 October 2023; (C) Haikui default and (D) Haikui 0.01× at 16:00 UTC on 6 September 2023. Red square in (A-B) marks the 600 × 600 km region around low-pressure center of Koinu; red square in (C-D) marks the 800 × 800 km region around low-pressure center of Haikui. (For interpretation of the references to colour in this figure legend, the reader is referred to the web version of this article.)

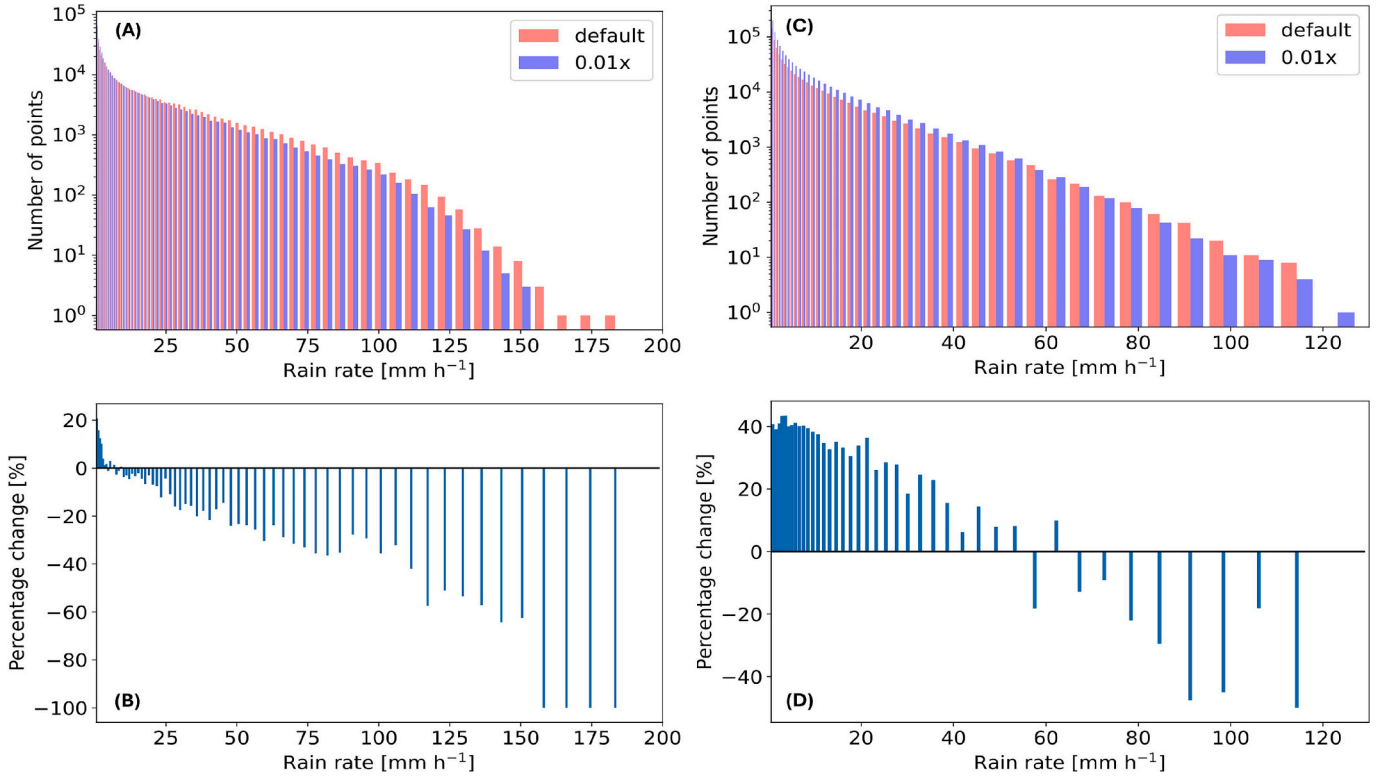

Fig. 6. (A-B) Number of grid points with rain rates exceeding 1 mm h^{-1} and their percentage changes from default to 0.01× conditions, binned by precipitation intensity (bin size increasing from 0.5 to 10 mm h^{-1}), averaged over the final 48 h across ensemble simulations for a 600 × 600 km region around Koinu's low-pressure center. (C-D) Corresponding results for an 800 × 800 km region around Haikui's low-pressure center.

is important to study the impacts of reduced aerosol concentration on the development of tropical cyclones to understand how this natural hazard may change in the future.

In this study, we employ the Weather Research and Forecasting (WRF) model (Skamarock et al., 2021) with Thompson aerosol-aware microphysics scheme (Thompson and Eidhammer, 2014) to assess the impact of reduced aerosol concentration on the development of precipitation of tropical cyclones in the South China region. Thompson aerosol-aware microphysics scheme is a bulk microphysics scheme that nucleates water and ice from their dominant respective nuclei and tracks and predicts the number of available aerosols (Thompson and Eidhammer, 2014). As a bulk scheme, the Thompson aerosol-aware scheme is less sensitive to aerosols than spectral bin microphysics schemes that calculate particle size distributions by solving explicit microphysical equations. This could be due to the application of saturation adjustment, which makes the scheme insensible to aerosols at the stage of diffusional growth, as well as errors in size sorting during sedimentation (Khain et al., 2016). Although this may modestly hinder the scheme's performance in simulating the evolution of tropical cyclone's intensity and structure, the Thompson aerosol-aware scheme offers a practical balance between accuracy and computational efficiency. Using less computational resources, it is capable of achieving similar performance as WRF-Chem, which includes more complex representation of aerosol properties, in simulating aerosol optical depths and aerosol impacts on near-storm environments (Saide et al., 2016). Among several other bulk microphysics schemes including NSSL 2-moment scheme with cloud condensation nuclei prediction, and Thompson microphysics and Morrison scheme with specified cloud drop concentration, Thompson aerosol-aware microphysics scheme gives results closest to those found in the observations and by using spectral bin microphysics in simulating Hurricane Irene in August 2011 (Khain et al., 2016). Given these advantages, we adopt the Thompson aerosol-aware scheme as a cost-effective yet sufficiently accurate method for investigating aerosol impacts in our study.

Our investigation involves simulations of Typhoon Haikui from 00 UTC on 4 September to 18 UTC on 8 September 2023 and Typhoon Koinu from 06 UTC on 5 October to 12 UTC on 9 October 2023. The two tropical cyclones were chosen because of the exceptionally high rainfall they brought. The periods across the highest precipitation in Hong Kong were chosen to simulate the extreme precipitation events and investigate how reduced aerosol amount would affect these impactful events. By analyzing how aerosol concentration alters microphysical processes, this research would provide insights into the validity and relative importance of warm-rain formation, cold-phase invigoration, or other mechanisms in determining the precipitation response of tropical cyclones to aerosol changes. Our study would also address the understudied but increasingly relevant scenario of future aerosol reductions.

2. Materials and methods

2.1. Cases

Our experiments are conducted with two tropical cyclone cases. The first is the case of Typhoon Haikui on 4–9 September 2023. After moving over Taiwan, Haikui made landfall in Fujian as a weakening tropical storm, but its remnant brought severe precipitation to Hong Kong, with a record-breaking 158.1 mm of rainfall in an hour recorded at the Hong Kong Observatory from local time 23:00 to midnight on 7 September. The second case is that of Typhoon Koinu on 5–9 October 2023. Koinu weakened after passing through the south of Taiwan, but re-strengthened as it moved across the South China Sea. The severe typhoon brought the highest ever 24-h rainfall in October to Hong Kong, which is 439.8 mm from local time 15:00 on 8 October to 15:00 the next day.

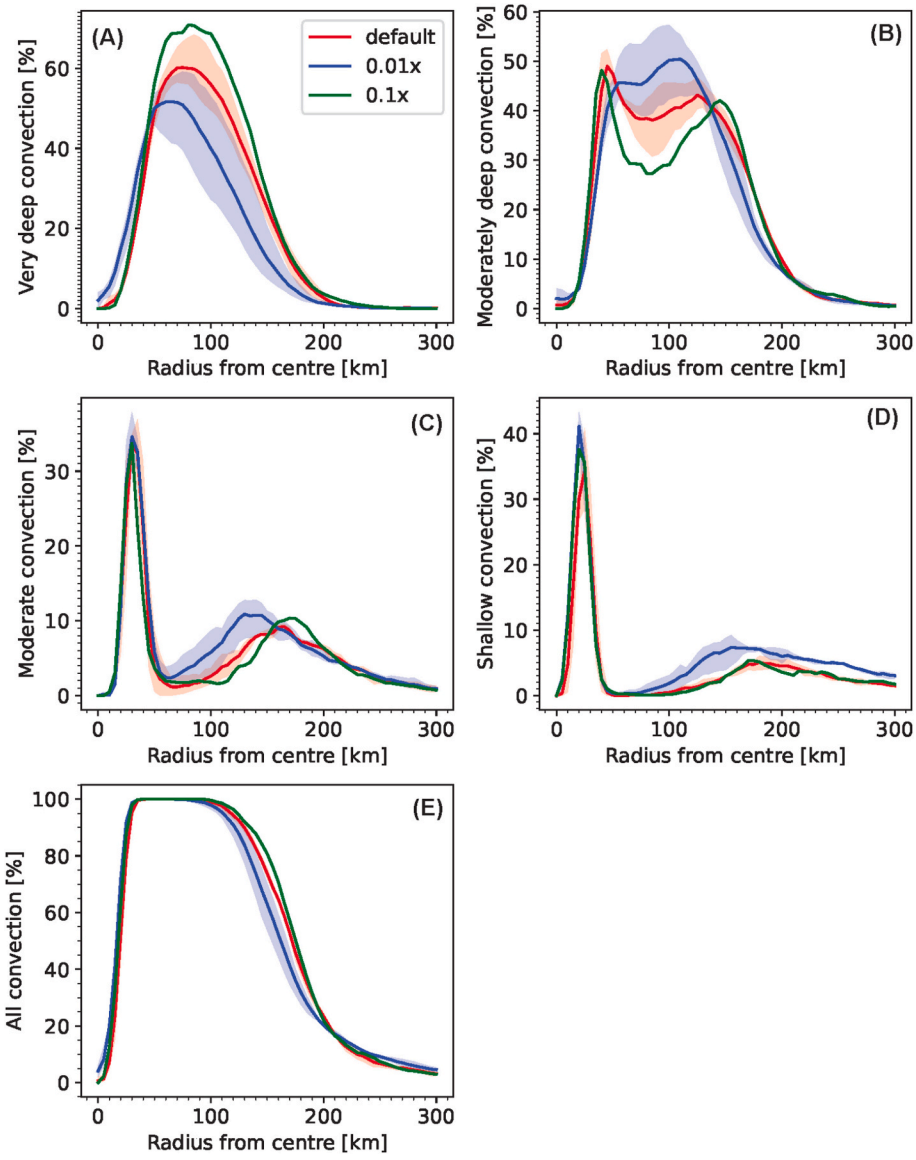

Fig. 7. Radial distributions of azimuthally averaged percent occurrence of (A) very deep, (B) moderately deep, (C) moderate, (D) shallow, and (E) all precipitation for Koinu averaged over the last 48 h of the simulation. Shaded regions mark the range of the results from the ensemble of three simulations.

2.2. Experiment design

The simulations were configured with three two-way nested domains centered at 22.3° N 113.8° E (see Fig. 1) with horizontal grid resolutions of 15, 5, and 1.67 km, respectively, using the WRF model version 4.5.1. The dimensions of the three domains are 3780 km × 3660 km, 2225 km × 1955 km and 1157 km × 1027 km. The vertical direction has 70 levels up to the model top at 50 hPa. The simulation for Haikui runs for 114 h from 00 UTC on 4 September 2023, while that for Koinu runs for 102 h from 06 UTC on 5 October 2023. Thompson aerosol-aware microphysics scheme was used in the simulations, which is a bulk microphysics scheme with explicit cloud droplet nucleation by water-friendly (WF) aerosols, which consists of sulfates, sea salts and organic matter, and ice activation by ice-friendly (IF) aerosols, which is primarily dust generated by natural wind erosion. The longwave and shortwave radiation schemes were both RRTMG, the land surface model was unified Noah, the surface layer scheme was QNSE, the Planetary Boundary Layer scheme was QNSE-EDMF, and Tiedtke cumulus parameterization scheme was applied to the largest domain.

The Thompson aerosol-aware microphysics scheme requires 3-dimensional aerosol number concentration data, which can be added to the metgrid output files following the steps outlined in https://www2.mmm.ucar.edu/wrf/users/physics/mp28_updated.html. The aerosol concentration data are derived from the global simulation of the Goddard Chemistry Aerosol Radiation and Transport (GOCART) model over 7 years (2001–2007) (Colarco et al., 2010; Thompson and Eidhammer, 2014), and these default values were used in our "default" experiment. From the column number concentration of organic carbon and sulfates calculated from the average column mass density of these species from September to October 2023 provided by MERRA-2 (Global Modeling and Assimilation Office (GMAO), 2015; Chin et al., 2002), the number concentration of these aerosols in the coast of South China is about two orders of magnitude larger than that in tropical Western Pacific Ocean (see Fig. 1). Therefore, to approximate the situation when aerosol concentration returns to the level when there were minimal human emission, the "0.01×" case is designed where WF aerosol concentration over the entire simulation domain was set to 0.01 times the default values by multiplying the variables "W_WIF" in the metgrid output files by 0.01. Although the IPCC SSP1–1.9 scenario projected only up to 10 times global aerosol emission reduction by 2100 (Chen et al., 2021), regions

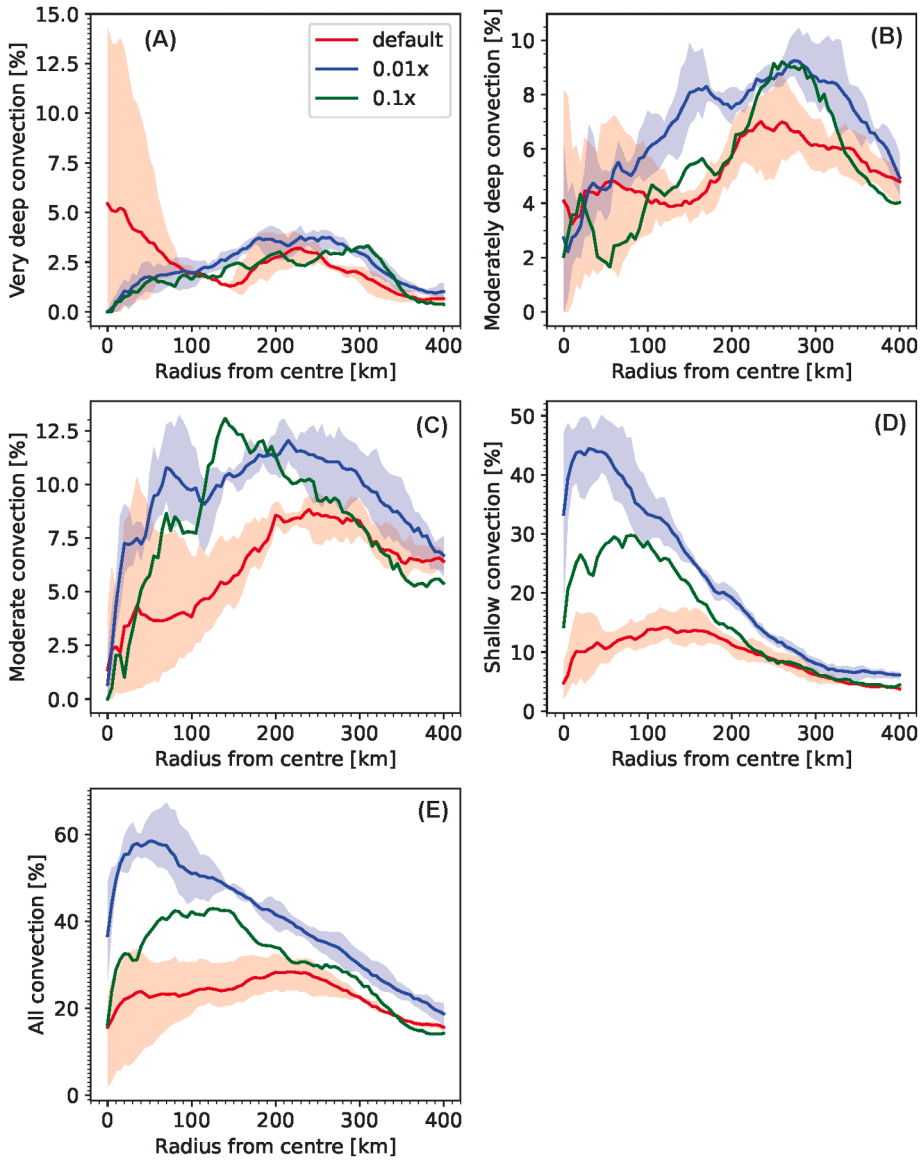

Fig. 8. Radial distributions of azimuthally averaged percent occurrence of (A) very deep, (B) moderately deep, (C) moderate, (D) shallow, and (E) all precipitation for Haikui averaged over the last 48 h of the simulation. Shaded regions mark the range of the results from the ensemble of three simulations.

such as South China and Southeast Asia, which currently emit far more aerosols than the global average, would need much deeper cuts to meet these targets. For instance, China alone contributes one-third of global SO_2 emissions and nearly a quarter of global organic carbon emissions (Crippa et al., 2024). Given these high baseline emissions, achieving SSP1–1.9 compliance in these regions would demand reductions on the order of 100 times, supporting the justification for the 100 times reduction in aerosols in our experiments. The IF aerosol concentration was kept constant in our experiments since it is not expected to change due to human activities. To further understand the effect when aerosol concentration is reduced but to a lesser extent, another simulation with 0.1 times the default WF aerosol concentration was carried out. Within the Thompson aerosol-aware microphysics scheme, aerosols are advected and diffused during the simulations, while surface emission is represented by a variable lower boundary condition (Thompson and Eidhammer, 2014) based on the initial near-surface aerosol concentration and a simple mean surface wind. This results in approximately 100 times/10 times reduction in surface emission when aerosol number concentration is reduced by 100 times/10 times.

The initial and boundary conditions of our simulations come from ECMWF Reanalysis V5 (ERA5) fields in 3-h intervals. Grid analysis nudging is applied to the largest domain every three hours. To ensure the robustness of the simulation results, for each tropical cyclone case, a small ensemble of three pairs of default and 0.01× simulations are carried out. Members of each ensemble differ by small perturbations at the lowest three levels of temperature fields, which are below 500 m, in the form of random noise with an amplitude of 0.001 K.

3. Results

3.1. Impacts on track and intensity

The simulated tracks of Koinu and Haikui determined by minimum sea level pressure are shown in Fig. 2. Koinu remained over the ocean for the entire simulation, while Haikui made landfall at around 21 h after the start of the simulation. Changes in aerosol concentration have little impact on the tracks of both typhoons, which is consistent with the findings of previous studies (Cotton et al., 2012; Hazra et al., 2013; Jiang et al., 2016; Pan et al., 2020). Although the simulated tracks show slight deviations from the observed tracks, this should not affect our analysis,

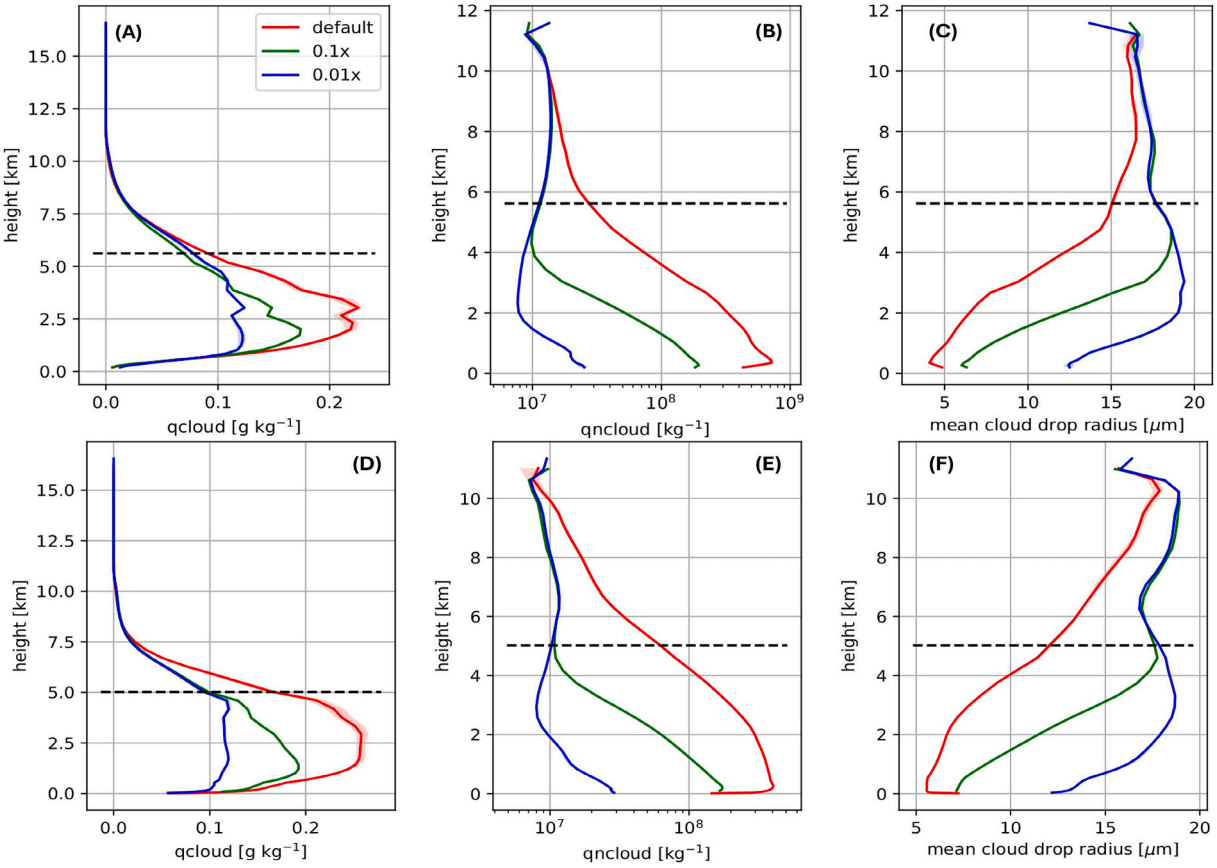

Fig. 9. Panels (A, D) show the mixing ratio of cloud droplets, (B, E) the number concentration of cloud droplets, and (C, F) the mean cloud droplet radius (assuming uniform droplet size) within cloudy regions (total liquid + ice content >0.1 g kg^{-1}). Results are averaged over the last 48 h of the simulation for (A–C) a 600 × 600 km region around Koinu's low-pressure center and (D-F) an 800 × 800 km region around Haikui's low-pressure center. Shaded areas indicate the ensemble spread from three simulations, and the dashed horizontal line marks the 0 °C level.

which focuses on comparison of aerosol effects.

The maximum surface wind speed and minimum sea level pressure of the two tropical cyclones are plotted in Fig. 3. It can be seen that Koinu continues to strengthen during the simulation, while Haikui weakens. The intensities of the two tropical cyclones change differently with aerosol concentration changes. For Koinu, reducing aerosol concentration initially strengthens the storm (maximum surface wind speed increases while minimum sea level pressure decreases), but the storm is weakened when aerosol concentration is further reduced to 0.01 times. Haikui shows only small difference in maximum surface wind speed for different aerosol concentrations, but shows lower minimum sea level pressure when aerosol concentration reduces.

3.2. Impacts on precipitation

Koinu and Haikui show different responses to reduced aerosol number concentration in terms of precipitation. Fig. 4 and Table 1 show the precipitation statistics in the 600 × 600 km region around low-pressure center of Koinu and the 800 × 800 km region around low-pressure center of Haikui. The region sizes were selected based on each typhoon's spatial characteristics to include their precipitation structures while excluding large non-precipitating areas. Fig. 4(A) and (C) show that mean precipitation around the low-pressure center of Koinu decreases with the reduction of aerosol number concentration, but increases for the case of Haikui. Considering the first 24 h of the simulation as spin-up and taking average over the rest of the simulation, the mean precipitation rate decreases from 1.55 mm h^{-1} to 1.42 mm h^{-1} for Koinu but increases from 1.07 mm h^{-1} to 1.22 mm h^{-1} for Haikui when aerosol number concentration is reduced by a factor of 100. Meanwhile, the area extent of precipitation is larger in cleaner conditions for both tropical cyclones as shown in Fig. 4(B) and (D). By applying one-sided Wilcoxon signed-rank test on the ensemble of simulations, it is confirmed that the differences described above are all statistically significant ($P < 0.05$). In Fig. 4, the green lines representing the simulation with aerosol number concentration reduced by a factor of 10 ("0.1×") do not always lie between the red and blue lines, representing the simulations with default concentration and concentration reduced by a factor of 100 ("0.01×"), highlighting the complex response of precipitation to changes in aerosol concentration. The non-monotonic response is particularly pronounced in the case of Koinu, which will be further discussed in Section 3.4.

Fig. 5 compares the composite radar reflectivity at two instants of Koinu and Haikui in one of the default and 0.01× simulations. This pair of images was chosen to illustrate the differences in precipitation pattern as there is a large difference in both mean non-zero precipitation and area fraction of precipitation at this instant. The distributions of precipitation regions in different realizations in an ensemble are similar in the first 24 h, though there are small variations in intensity. As the simulations progress, the distributions of precipitation regions among different realizations diverge in addition to the intensity. However, reflectivity patterns in default and 0.01× runs differ from the beginning of the simulations, with 0.01× runs having noticeably larger areas with reflectivity lower than 30 dBZ. This is consistent with the results shown in Fig. 4(B) and (D).

For the case of Koinu, since mean precipitation rate decreases while area of precipitation increases when aerosol reduces, rainfall intensity in cleaner conditions decreases significantly. From Table 1, the mean rain rate in regions with precipitation exceeding 0.01 mm h^{-1} decreases from

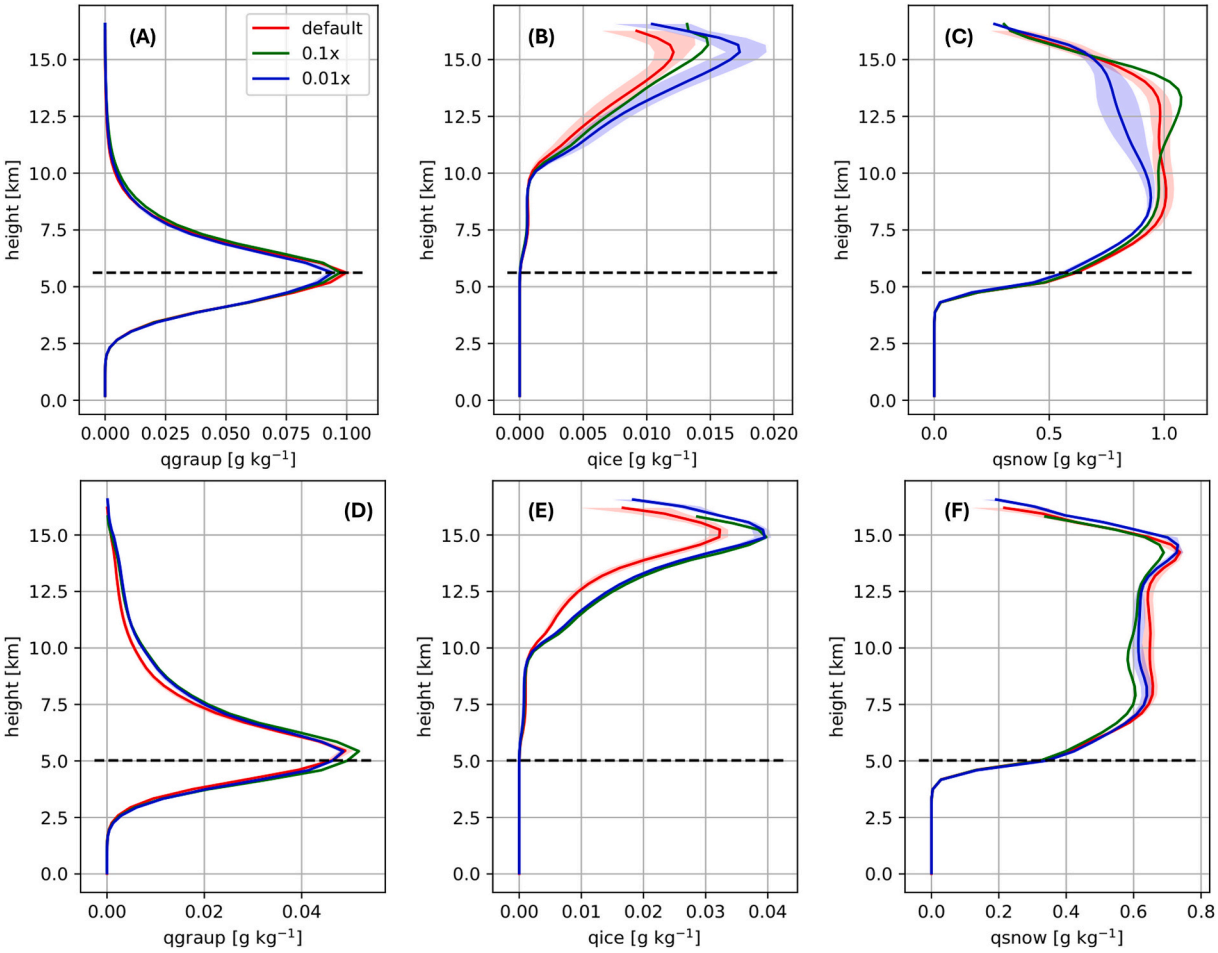

Fig. 10. (A-C) Mixing ratios of graupel, ice and snow within cloudy regions (total liquid + ice content >0.1 g kg^{-1}). Results are averaged over the last 48 h of the simulation for (A-C) a 600 × 600 km region around Koinu's low-pressure center and (D-F) an 800 × 800 km region around Haikui's low-pressure center. Shaded areas indicate the ensemble spread from three simulations, and the dashed horizontal line marks the 0 °C level.

4.07 mm h^{-1} to 3.21 mm h^{-1} when aerosol number concentration decreases by a factor of 100. From Fig. 5(A) and (B), higher precipitation intensity can be found in the eyewall region of Koinu in the default case, while more small patches of low to moderate precipitation are found at the periphery for the 0.01× case. Although the overall mean precipitation rate exhibits an opposite trend for Haikui, rainfall intensity in precipitating areas is still found to decrease slightly when aerosol number concentration reduces as reflected by the statistics shown in Table 1. Fig. 5(C) and (D) show the maximum radar reflectivity at 16:00 UTC on 6 September 2023 from the default and 0.01× simulation of Haikui respectively. As Haikui had already made landfall at around 21:00 UTC on 4 September 2023, the structure of the typhoon is no longer well-defined. Nonetheless, it is evident that the precipitation area in the 0.01× simulation is much more extensive, and it mainly consists of precipitation with low to moderate intensity. Although there are also patches with more intense precipitation (radar reflectivity above 45 dBZ) in the 0.01× simulation, the intensity is not as high as the strongest precipitation in the default simulation, which involves radar reflectivity above 55 dBZ. It is also worth noting that away from the tropical cyclones, the unorganized convective cells also show significant difference between the default and 0.01× simulations, with the 0.01× simulations having larger convective regions.

Fig. 6(A) and (C) show the distributions of rain rate around the low-pressure centers of Koinu and Haikui, and Fig. 6(B) and (D) show the percentage change from default to 0.01× simulations. In Koinu, when aerosol concentration decreases, the number of points with low rain rate of less than 6 mm h^{-1} increases, while the number of points with moderate to high rain rate decreases. In particular, the high aerosol runs have extreme precipitation of above 150 mm h^{-1}, while the clean runs do not. In Haikui, the maximum precipitation is about 55 mm h^{-1} lower than in Koinu, but the 0.01× simulations have more points with rain rate up to 50 mm h^{-1}. Above 50 mm h^{-1}, the 0.01× simulations still have fewer number of points in general, similar to the case in Koinu. Meanwhile, the percentage decrease in the number of points with high rain rate is higher for Koinu than in Haikui, while the percentage increase in the number of points with low rain rate is higher for Haikui than in Koinu. From these, we can see that the difference in precipitation in Koinu is likely mainly due to changes in processes that generate moderate to intense precipitation, while the difference in precipitation in Haikui is likely mainly due to changes in processes that generate light to moderate rain.

This is further supported by Figs. 7 and 8, which show the radial distributions of different types of precipitation defined using the 20-dBZ radar echo height (Z_{20dBZ}) according to Tao and Jiang (2015) averaged over the last 48 h of the simulations. From Fig. 7, the rain band of Koinu at 40–180 km from the tropical cyclone center is dominated by very deep ($Z_{20dBZ} \geq 14$ km) and moderately deep ($14 > Z_{20dBZ} \geq 10$ km) precipitation. When aerosol concentration reduces, the percent occurrence of very deep precipitation at 40–180 km from the tropical cyclone center reduces, while that of moderately deep, moderate ($10 > Z_{20dBZ} \geq 6$ km) and shallow ($Z_{20dBZ} < 6$ km) precipitation in the same region increases, suggesting a reduction in convective strength. Beyond 200 km from the center of Koinu, percent occurrence of shallow precipitation increases. From Fig. 7(E), the percent occurrence of total precipitation is

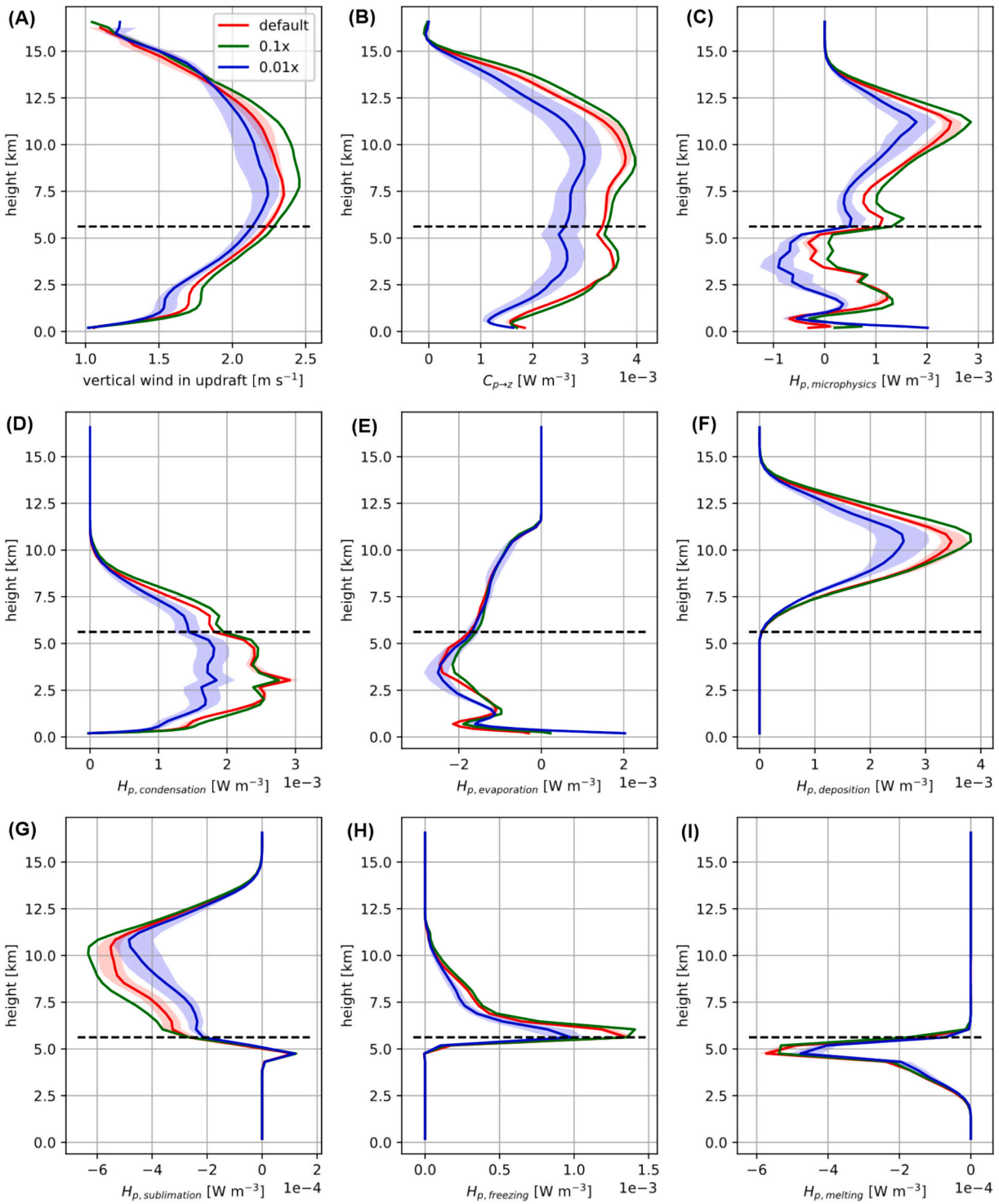

Fig. 11. Vertical profiles computed in 600 × 600 km region around low-pressure center of Koinu averaged over the last 48 h of the simulation. (A) Vertical velocity in cloudy updraft regions with $w > 1$ m s^{-1} and total liquid and ice content above 0.1 g kg^{-1} (B) Conversion from MAPE to vertical kinetic energy $C_{p\to z}$ (C) Sum of diabatic contribution due to microphysical processes (D-I) Diabatic contribution H_p due to condensation, evaporation, deposition, sublimation, freezing and melting. Shaded regions mark the range of the results from the ensemble of three simulations. Dashed horizontal line denotes the 0 °C level.

almost the same at different aerosol levels. At a radial distance of 100–200 km, more polluted runs have larger precipitation area, but beyond 200 km, the cleaner runs have slightly larger precipitation area.

On the other hand, Fig. 8(E) shows significant increase in percent occurrence of total precipitation in Haikui at all radial distances when aerosol concentration reduces, suggesting significant expansion in precipitation area. The change is dominated by increase in shallow precipitation as displayed in Fig. 8(D). There is no significant difference in the percent occurrence of moderate, moderately deep, and very deep convection for different aerosol levels for Haikui (only around 2 % difference). The contributions from moderate to very deep convection are also limited since their percent occurrences are significantly lower than that in Koinu. This is as expected since Haikui made landfall and was dissipating, while Koinu remained over the ocean, its energy source,

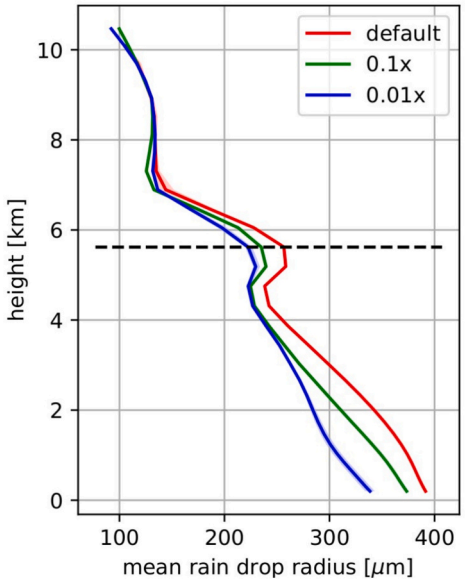

Fig. 12. Mean rain radius (assuming uniform droplet size) within regions with rain mixing ratio > 0.1 g kg^{-1} averaged over the last 48 h of the simulation for a 600 × 600 km region around Koinu's low-pressure center. Shaded areas indicate the ensemble spread from three simulations, and the dashed horizontal line marks the 0 °C level.

throughout the simulation.

3.3. Microphysical processes

To understand the differences in percent occurrence of various kinds of precipitation-convection, we look deeper into the microphysical processes that could influence precipitation and convective strength. In this section, we first focus on the comparison between the default and 0.01× scenarios, while the results of the 0.1× scenario will be discussed in the next section.

First, changes in shallow precipitation can be explained by the well-established theory on how aerosol concentration affects warm-cloud precipitation (e.g. Rosenfeld et al. (2008); Tao et al. (2012)). When aerosol number concentration is lower, fewer but larger cloud droplets are formed as shown in Fig. 9(B,E) and (E,F). Since larger droplets collide more efficiently, the formation of warm-cloud precipitation is promoted, leading to a decrease in cloud water mass from default to clean runs as shown in Fig. 9(A) and (D). On the other hand, high concentration of cloud condensation nuclei would result in smaller cloud droplets. Although the number of droplets would be higher, they collide less effectively due to smaller cross-sectional areas and hence do not form warm rain effectively. This could explain the increase in shallow precipitation for both Koinu and Haikui when aerosol concentration reduces, and why larger areas with less intense precipitation are observed in clean simulations in both tropical cyclones. Since precipitation in Haikui is mostly contributed by shallow convection, this effect is also the main reason that there is higher overall rainfall in Haikui in cleaner simulations. Whereas in Koinu, shallow precipitation is not the dominating precipitation type at 40–180 km from the tropical cyclone center, so the above process cannot explain its overall precipitation response to aerosol changes. Rather, we need to look at other processes that could influence convection strength and convective precipitation.

In Koinu, vertical velocity in updrafts is generally higher in default runs compared to the cleanest runs at both lower and upper levels, which could result in deeper convection in default runs. While aerosols do not directly influence updraft velocity, they can modify rates of microphysical processes, which determine the amount of latent heat released or absorbed, thereby influencing buoyancy and ultimately updraft strength. Therefore, to understand how aerosol concentration changes result in changes in convection depth observed, we look into the microphysical processes that generate buoyancy and how effectively the potential energy converts into kinetic energy in updrafts.

According to Peng et al. (2014), in a fully compressible, non-hydrostatic, moist atmosphere, moist available potential energy (MAPE) can be defined to quantify the small, active portion of potential energy in a moist atmosphere that is available to be converted into kinetic energy. Using the modified potential temperature $\theta_m = \theta\left(1+\frac{R_v}{R_d}q_v\right) \approx \theta(1+1.61q_v)$, where θ is the potential temperature, R_d is the gas constant for dry air, R_v is the gas constant for water vapor and q_v is the water vapor mixing ratio, MAPE per unit mass is defined as

$$E_p = \frac{g^2}{2N^2\overline{\theta}^2}\theta_m'^{\,2}, \tag{1}$$

where g is the gravitational constant and $N^2 = g\partial\ \ln\overline{\theta}/\partial z$ is the Brunt-Väisälä frequency. The overline denotes the time-invariant, hydrostatically balanced, dry reference state, which is taken as the mean state of the atmosphere at the start of the simulations following the method in Harris et al. (2022). The prime (′) denotes the perturbation from the reference state. The budget equation of MAPE is given by (Peng et al., 2015)

$$\frac{\partial}{\partial t}\left(\rho_d E_p\right) = A_p - C_{p\to z} + H_p + D_p + N_p \tag{2}$$

where A_p is the advection term, $C_{p\to z} = \rho_d g w\theta_m'/\overline{\theta}$denotes the conversion from MAPE to vertical kinetic energy, $H_p = \frac{g^2}{N^2\overline{\theta}^2}\rho_d\theta_m' H_m$ is the diabatic heating term, D_p is the diffusion term, and N_p is the nonlinear term. ρ_d is the density of dry air, w is the vertical wind, and $H_m = (1+1.61q_v)S_\theta + 1.61\theta S_{q_v}$ is the combined diabatic influence with S_θ and S_{qv} being the diabatic contributions to potential temperature and water vapor respectively. In tropical cyclones, the MAPE budget is dominated by H_p and $C_{p\to z}$ (Wu et al., 2024), while the other terms are negligible. In addition, within the H_p term, contribution from microphysical processes dominates over PBL contribution related to sensible heat flux transportation (Wu et al., 2024). Therefore, we will focus on the diabatic contribution due to microphysics and conversion from MAPE to vertical kinetic energy in the following analysis.

The vertical profiles of the different terms for Koinu are shown in Fig. 11. In Koinu, the condensation term (Fig. 11(D)) is higher in the default scenario because there are more cloud condensation nuclei, so more MAPE is generated by condensation. From Fig. 9(A), more cloud water is present at lower levels in the default scenario, and those cloud droplets are smaller in size than in the 0.01× scenario (see Fig. 9(C)) since there are more cloud condensation nuclei. One would expect that the evaporation term to be more negative in the default run, but Fig. 11 (E) shows that it is slightly less negative than in the clean run. This is likely because in the default run, the larger percent occurrence of moderately deep to very deep convection produces raindrops that are larger in size as shown in Fig. 12. Since larger raindrops have lower surface-area-to-volume ratios, this decreases evaporation efficiency, leading to less negative H_p term for evaporation at lower levels in a more polluted environment. At higher levels, although in a more polluted environment, warm rain forms less efficiently by autoconversion of smaller cloud droplets, resulting in more droplets to be brought upwards to upper levels, the difference in evaporation between default and clean runs is found to be small because the additional droplets turned into ice, snow or graupel quickly. Therefore, the amount of supercooled liquid present in default and clean scenarios do not differ greatly. This is supported by Fig. 9(A), which shows that cloud water mixing ratio in the mixed layer just above the 0 °C level is similar in the default and the 0.01× scenarios.

Meanwhile, Fig. 10(C) shows that there is a larger snow mixing ratio

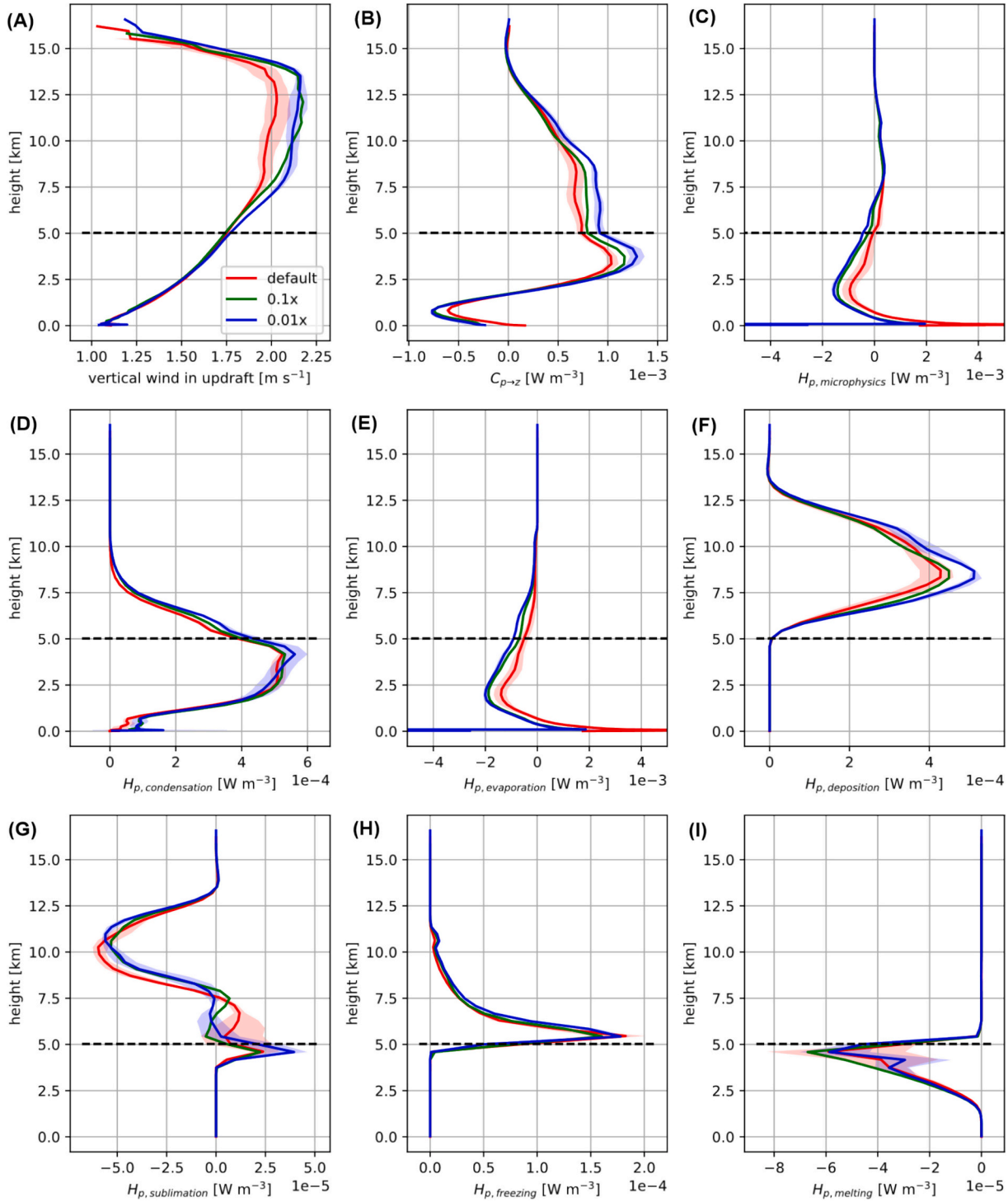

Fig. 13. Vertical profiles computed in 800 × 800 km region around low-pressure center of Haikui averaged over the last 48 h of the simulation. (A) Vertical velocity in cloudy updraft regions with $w > 1$ m s^{-1} and total liquid and ice content above 0.1 g kg^{-1} (B) Conversion from MAPE to vertical kinetic energy $C_{p\to z}$ (C) Sum of diabatic contribution due to microphysical processes (D-I) Diabatic contribution H_p due to condensation, evaporation, deposition, sublimation, freezing and melting. Shaded regions mark the range of the results from the ensemble of three simulations. Dashed horizontal line denotes the 0 °C level.

in the default scenario. The clean scenario has more ice near the cloud top (see Fig. 10(B)), which is probably because in the default scenario, more ice crystals have been converted into snow or graupel by collecting water droplets. Indeed, both deposition and freezing terms (Fig. 11(F) and (H)) are more positive in the default scenario, which shows that there are more deposition and freezing in convective cores due to more supercooled liquid brought above the freezing level. Although the sublimation and melting terms (Fig. 11(G) and (I)) are more negative in the default scenario, their magnitudes are small compared to the deposition and freezing terms, so they only destroy a small portion of the MAPE generated by deposition and freezing. Overall, microphysical processes in a less clean environment generate more MAPE as shown in Fig. 11(C). In addition, the $C_{p\to z}$ term (Fig. 11(B)) of the default scenario is larger than the 0.01× scenario, which means more MAPE is converted into vertical kinetic energy to drive convection in a more polluted environment. As a result, the updraft velocity in a default scenario is higher

(Fig. 11(A)) and convection is stronger and deeper. Through mass continuity principles, these enhanced vertical motions necessitate compensatory intensification of the low-level inflow, which explains the stronger surface wind speed of Koinu in the default scenario as shown in Fig. 3(A). The strong radial inflow transports greater quantities of cloud droplets into the convective cores, initiating a positive feedback cycle wherein the increased droplet influx brings more supercooled liquid water to higher altitudes where they freeze and release latent heat, further intensifying updrafts and deepening the convection. Ultimately, this self-reinforcing mechanism explains the more intense precipitation seen in the default scenario.

In Haikui, for all microphysical processes, the amount of MAPE generated or destroyed illustrated in Fig. 13(D-I) are small compared to that in Koinu, especially for ice processes. The differences between default and clean scenarios are also small. Total diabatic forcing due to microphysics (Fig. 13(C)) is small and even negative below the freezing level due to more evaporation than condensation. In addition, $C_{p\rightarrow z}$ is small and even negative below 2 km (see Fig. 13(B)), which is as expected since the typhoon is dissipating. These suggest that low-level updraft in Haikui is not thermally driven by latent heating of microphysical processes, but is mostly mechanically driven instead. This is likely the case since Haikui has made landfall and experiences more surface friction as opposed to Koinu which remained over the ocean. As a result, as shown in Fig. 13(A), changes in aerosol number concentration do not result in significant difference in low-level updraft strength in Haikui. Moreover, in the clouds of Haikui, there is less deposition and freezing than in the clouds of Koinu, resulting in less snow and graupel, which is evident by comparing the values in Fig. 10(A,D) and (C,F). Therefore, the precipitation in Haikui is primarily due to warm rain produced in shallow clouds instead of rain formed by the melting of falling graupel or snow formed in deep convective clouds. As a result, in a cleaner scenario, Haikui has higher overall rainfall because of more warm rain formed by higher collision efficiency of fewer but larger cloud droplets, but does not suffer from the precipitation suppression due to suppression of invigoration compared to the default case as in Koinu. Without significant difference in updraft strengths, the surface wind speed in Haikui shown in Fig. 3(C) also does not show significant difference across different aerosol concentration levels.

3.4. Monotonicity of trends

From Fig. 4, it can be observed that the response of the three sets of simulations with different aerosol number concentration is less prominent and less monotonic for Koinu than for Haikui. A possible reason is that for Koinu, cold processes compete over the warm rain process in affecting the formation of precipitation. Since these processes have opposing effects on precipitation amount, the net precipitation is determined by how much one process outweighs the other, which is non-trivial. On the other hand, for Haikui, since the warm rain process dominates, the increase in precipitation with decreasing aerosol number concentration is more prominent and monotonic.

In addition, from Fig. 10(C), the 0.1× experiment with intermediate aerosol concentration has the largest snow mixing ratio at upper levels, while the default experiment has slightly lower value. This is in agreement with Cotton et al. (2012) and Hazra et al. (2013), which found that mixing ratios of ice hydrometeors initially increase with increasing pollutant concentration, but there is a "tipping point" after which further increase in aerosol concentration reduces droplet sizes so much that riming is suppressed, resulting in smaller frozen particles that are less likely to fall out by precipitation. Therefore, the default experiments may show slightly less precipitation than the 0.1× experiment.

4. Discussion

Aerosol emission is expected to be reduced in the future with increasing emission reduction policies to mitigate climate change. This study demonstrates that future reductions in water-friendly aerosols may significantly alter tropical cyclone precipitation patterns in the South China region. Through simulations of Typhoons Haikui and Koinu using the Thompson aerosol-aware microphysics scheme, we identified two key consistent responses to aerosol reduction: an expansion of precipitation area due to enhanced warm-rain processes, and case-dependent intensity changes tied to storm characteristics. The dissipating Haikui showed minimal changes in updraft strength with aerosol reduction, as its precipitation remained dominated by warm-rain processes with limited ice-phase contributions. In contrast, the strengthening Koinu exhibited weaker convection and less intense precipitation in cleaner environments, resulting from reduced diabatic heating due to ice-phase processes and less efficient conversion of potential energy into vertical kinetic energy, suggesting that aerosol cold-phase invigoration is present in Koinu.

These results are largely consistent with those of recent research. The enhancement of precipitation due to warm-rain processes and the reduced convective precipitation due to suppressed ice-phase processes in a cleaner atmosphere were found in different tropical cyclone environments. For instance, many studies using different microphysics schemes (e.g. Cotton et al. (2012) using advanced two-moment bin-emulating microphysics scheme, Hazra et al. (2013) using bulk microphysics scheme with condensation nuclei initialized with trimodal lognormal size distributions, and Jiang et al. (2016) using WRF-CHEM with two-moment bulk microphysics scheme) have found more precipitation in a cleaner environment due to more efficient collision-coalescence. Meanwhile, depending on the characteristics of the tropical cyclone, convective invigoration due to increased aerosols occurs at different times or locations within tropical cyclones (Cotton et al., 2012; Herbener et al., 2014; Jiang et al., 2016), or to different extents depending on whether the "tipping point" is reached (Hazra et al., 2013; Cotton et al., 2012) resulting in different precipitation patterns.

Our findings have important implications for climate modeling and policy. The robust expansion of precipitation area suggests that future emission reductions may systematically increase the spatial footprint of tropical cyclone rainfall, even when intensity responses vary. This underscores the need to incorporate realistic aerosol projections, such as those by Li et al. (2022), into climate models to improve precipitation forecasts. For policymakers, our results highlight that emission reduction strategies should account for potential changes in tropical cyclone hydrology, particularly in vulnerable coastal regions. However, broader conclusions would benefit from analysis of a larger sample of tropical cyclones across varying intensities, tracks, and environmental conditions to establish generalizable patterns.

Our analysis focused specifically on aerosol-cloud interactions, and we found aerosol-radiation effects are comparatively minor in these systems. Radiative tendencies in our simulations were consistently 13–23 times smaller than latent heating tendencies, with changes across aerosol scenarios being 27–36 times less significant for radiation than for latent heating. This substantial difference justifies our primary focus on microphysical rather than radiative aerosol effects in tropical cyclone precipitation. However, in regions such as India where atmospheric brown cloud composed of black and organic carbon aerosols is present, aerosol radiative effects would likely play a larger role, and the combined effects of microphysics and radiation should be considered.

Several limitations warrant consideration in interpreting our results. The Thompson aerosol-aware scheme's use of saturation adjustment may overestimate cloud buoyancy by neglecting negative feedback between supersaturation and updraft strength (Grabowski and Morrison, 2016), while inherent uncertainties in ice-microphysics parameterizations (Varble et al., 2023) affect the simulation of cold-phase processes. Although ensemble simulations confirmed the robustness of precipitation area changes, future work should employ multi-model comparisons (e.g., Iguchi et al. (2020); Khain et al. (2016)) and innovative methodologies like microphysical piggybacking (Grabowski (2014, 2015); Grabowski and Morrison (2020); Sarkadi et al. (2022)) to better isolate

microphysical-dynamical feedbacks. Additional simulations with more gradual aerosol reductions would also be valuable for properly characterizing response linearity. Furthermore, investigating different anthropogenic aerosols with diverse chemical compositions, sizes, and nucleation activity could provide valuable insights into their specific impacts on tropical cyclone precipitation. Such approaches, applied to diverse tropical cyclone cases, will be crucial for developing more reliable projections of how aerosol reductions may modify tropical cyclone impacts in a changing climate.

CRediT authorship contribution statement

Ho Yi Lydia Mak: Writing – review & editing, Writing – original draft, Visualization, Methodology, Investigation, Formal analysis. **Yi Zhang:** Writing – review & editing, Investigation. **Xiaoming Shi:** Writing – review & editing, Supervision, Methodology, Funding acquisition, Conceptualization.

Declaration of competing interest

Authors declare that they have no competing interests.

Acknowledgments

The work described in this paper was substantially supported by a grant from the Research Grants Council (RGC) of the Hong Kong Special Administrative Region, China (Project Reference Number: AoE/P-601/23-N). XS is also supported by the RGC grant HKUST-16307323. The authors thank HKUST Fok Ying Tung Research Institute and the National Supercomputing Center in Guangzhou Nansha sub-center for providing high-performance computational resources.

Data availability

The Weather Research and Forecast model is publicly available at https://github.com/wrf-model/WRF. The ERA5 reanalysis data is available in the Copernicus Climate Change Service (C3S) Climate Data Store (https://cds.climate.copernicus.eu). We archived the namelist for our simulations at https://doi.org/10.5281/zenodo.11183306.

References

Andreae, M.O., Rosenfeld, D., Artaxo, P., Costa, A.A., Frank, G., Longo, K.M., Silva-Dias, M.A.F.d., 2004. Smoking rain clouds over the Amazon. Science 303, 1337–1342.

Chen, D., Rojas, M., Samset, B., Cobb, K., Diongue Niang, A., Edwards, P., Emori, S., Faria, S., Hawkins, E., Hope, P., Huybrechts, P., Meinshausen, M., Mustafa, S., Plattner, G.K., Tréguier, A.M., 2021. Framing, context, and methods. In: Masson-Delmotte, V., Zhai, P., Pirani, A., Connors, S.L., Péan, C., Berger, S., Caud, N., Chen, Y., Goldfarb, L., Gomis, M.I., Huang, M., Leitzell, K., Lonnoy, E., Matthews, J. B.R., Maycock, T.K., Waterfield, T., Yelekçi, O., Yu, R., Zhou, B. (Eds.), Climate Change 2021: The Physical Science Basis. Contribution of Working Group I to the Sixth Assessment Report of the Intergovernmental Panel on Climate Change. Cambridge University Press, Cambridge, UK and New York, NY, USA. https://doi.org/10.1017/9781009157896.003 book section 1.

Chin, M., Ginoux, P., Kinne, S., Torres, O., Holben, B.N., Duncan, B.N., Martin, R.V., Logan, J.A., Higurashi, A., Nakajima, T., 2002. Tropospheric aerosol optical thickness from the GOCART model and comparisons with satellite and sun photometer measurements. J. Atmos. Sci. 59, 461–483.

Colarco, P., da Silva, A., Chin, M., Diehl, T., 2010. Online simulations of global aerosol distributions in the NASA GEOS-4 model and comparisons to satellite and ground-based aerosol optical depth. J. Geophys. Res. Atmos. 115.

Cotton, W., Krall, G., Carrió, G., 2012. Potential indirect effects of aerosol on tropical cyclone intensity: convective fluxes and cold-pool activity. Trop. Cyclone Res. Rev. 1, 293–306.

Crippa, M., Guizzardi, D., Pagani, F., Banja, M., Muntean, M., Schaaf, E., Becker, W., Ferrario, F.M., Quadrelli, R., Martin, A.R., Grassi, G., Rossi, S., De Melo, J.B., Oom, D.J.F., Branco, A., San-Miguel, J., Vignati, E., 2024. https://edgar.jrc.ec.europa.eu/dataset_ap81.

Fan, J., Khain, A., 2021. Comments on "Do ultrafine cloud condensation nuclei invigorate deep convection?". J. Atmos. Sci. 78, 329–339.

Fan, J., Rosenfeld, D., Zhang, Y., Giangrande, S.E., Li, Z., Machado, L.A., Martin, S.T., Yang, Y., Wang, J., Artaxo, P., et al., 2018. Substantial convection and precipitation enhancements by ultrafine aerosol particles. Science 359, 411–418.

Global Modeling and Assimilation Office (GMAO), 2015. MERRA-2 tavg1 2d_aer_Nx: 2d, 1-Hourly, Time-averaged, SingleLevel,Assimilation, Aerosol Diagnostics V5.12.4. https://doi.org/10.5067/KLICLTZ8EM9D accessed: 2024-03-26.

Grabowski, W.W., 2014. Extracting microphysical impacts in large-eddy simulations of shallow convection. J. Atmos. Sci. 71, 4493–4499.

Grabowski, W.W., 2015. Untangling microphysical impacts on deep convection applying a novel modeling methodology. J. Atmos. Sci. 72, 2446–2464.

Grabowski, W.W., Morrison, H., 2016. Untangling microphysical impacts on deep convection applying a novel modeling methodology. Part II: Double-moment microphysics. J. Atmos. Sci. 73, 3749–3770.

Grabowski, W.W., Morrison, H., 2020. Do ultrafine cloud condensation nuclei invigorate deep convection? J. Atmos. Sci. 77, 2567–2583.

Harris, B.L., Tailleux, R., Holloway, C.E., Vidale, P.L., 2022. A moist available potential energy budget for an axisymmetric tropical cyclone. J. Atmos. Sci. 79, 2493–2513.

Hazra, A., Goswami, B., Chen, J.P., 2013. Role of interactions between aerosol radiative effect, dynamics, and cloud microphysics on transitions of monsoon intraseasonal oscillations. J. Atmos. Sci. 70, 2073–2087.

Herbener, S.R., Van Den Heever, S.C., Carrió, G.G., Saleeby, S.M., Cotton, W.R., 2014. Aerosol indirect effects on idealized tropical cyclone dynamics. J. Atmos. Sci. 71, 2040–2055.

Hong Kong Observatory, 2024. The Year's Weather – 2023. https://www.hko.gov.hk/en/wxinfo/pastwx/2023/ywx2023.htm.

Hong Kong Observatory, 2024a. Tropical Cyclones in 2023 > Six-Hourly Position and Intensity Data of Severe Typhoon Haikui (2311). URL. https://www.hko.gov.hk/en/publica/tc/tc2023/six_hrly_data_haikui.html.

Hong Kong Observatory, 2024b. Tropical Cyclones in 2023 > Six-Hourly Position and Intensity Data of Severe Typhoon Koinu (2314). URL. https://www.hko.gov.hk/en/publica/tc/tc2023/six_hrly_data_koinu.html.

Huang, R.J., Zhang, Y., Bozzetti, C., Ho, K.F., Cao, J.J., Han, Y., Daellenbach, K.R., Slowik, J.G., Platt, S.M., Canonaco, F., et al., 2014. High secondary aerosol contribution to particulate pollution during haze events in China. Nature 514, 218–222.

Iguchi, T., Rutledge, S.A., Tao, W.K., Matsui, T., Dolan, B., Lang, S.E., Barnum, J., 2020. Impacts of aerosol and environmental conditions on maritime and continental deep convective systems using a bin microphysical model. J. Geophys. Res.-Atmos. 125, e2019JD030952.

Jiang, B., Huang, B., Lin, W., Xu, S., 2016. Investigation of the effects of anthropogenic pollution on typhoon precipitation and microphysical processes using WRF-Chem. J. Atmos. Sci. 73, 1593–1610.

Jiang, B., Lin, W., Li, F., Chen, J., 2019. Sea-salt aerosol effects on the simulated microphysics and precipitation in a tropical cyclone. J. Meteorol. Res. 33, 115–125.

Khain, A., Rosenfeld, D., Pokrovsky, A., 2005. Aerosol impact on the dynamics and microphysics of deep convective clouds. Q. J. R. Meteorol. Soc. 131, 2639–2663.

Khain, A., Lynn, B., Shpund, J., 2016. High resolution WRF simulations of Hurricane Irene: Sensitivity to aerosols and choice of microphysical schemes. Atmos. Res. 167, 129–145.

Koren, I., Kaufman, Y.J., Rosenfeld, D., Remer, L.A., Rudich, Y., 2005. Aerosol invigoration and restructuring of Atlantic convective clouds. Geophys. Res. Lett. 32.

Koren, I., Feingold, G., Remer, L.A., 2010. The invigoration of deep convective clouds over the Atlantic: aerosol effect, meteorology or retrieval artifact? Atmos. Chem. Phys. 10, 8855–8872.

Li, H., Yang, Y., Wang, H., Wang, P., Yue, X., Liao, H., 2022. Projected aerosol changes driven by emissions and climate change using a machine learning method. Environ. Sci. Technol. 56, 3884–3893.

Liu, H., Tang, X., Gu, J.F., 2022. Effects of volcanic aerosols on the genesis of tropical cyclone Wukong (2018). J. Geophys. Res. Atmos. 127, e2022JD036775.

Pan, B., Wang, Y., Logan, T., Hsieh, J.S., Jiang, J.H., Li, Y., Zhang, R., 2020. Determinant role of aerosols from industrial sources in Hurricane Harvey's catastrophe. Geophys. Res. Lett. 47, e2020GL090014.

Peng, J., Zhang, L., Luo, Y., Xiong, C., 2014. Mesoscale energy spectra of the mei-yu front system. Part II: Moist available potential energy spectra. J. Atmos. Sci. 71, 1410–1424.

Peng, J., Zhang, L., Zhang, Y., 2015. On the local available energetics in a moist compressible atmosphere. J. Atmos. Sci. 72, 1551–1561.

Rosenfeld, D., Lohmann, U., Raga, G.B., O'Dowd, C.D., Kulmala, M., Fuzzi, S., Reissell, A., Andreae, M.O., 2008. Flood or drought: how do aerosols affect precipitation? Science 321, 1309–1313.

Rosenfeld, D., Woodley, W.L., Khain, A., Cotton, W.R., Carrió, G., Ginis, I., Golden, J.H., 2012. Aerosol effects on microstructure and intensity of tropical cyclones. Bull. Am. Meteorol. Soc. 93, 987–1001.

Saide, P.E., Thompson, G., Eidhammer, T., da Silva, A.M., Pierce, R.B., Carmichael, G.R., 2016. Assessment of biomass burning smoke influence on environmental conditions for multiyear tornado outbreaks by combining aerosol-aware microphysics and fire emission constraints. J. Geophys. Res. Atmos. 121, 10–294.

Sajjad, M., Chan, J.C., 2020. Tropical cyclone impacts on cities: a case of Hong Kong. Front. Built Environ. 6, 575534.

Sarkadi, N., Xue, L., Grabowski, W.W., Lebo, Z.J., Morrison, H., White, B., Fan, J., Dudhia, J., Geresdi, I., 2022. Microphysical piggybacking in the Weather Research and forecasting model. J. Adv. Model. Earth Syst. 14, e2021MS002890.

Skamarock, W.C., Klemp, J.B., Dudhia, J., Gill, D.O., Liu, Z., Berner, J., Wang, W., Powers, J.G., Duda, M.G., Barker, D.M., Huang, X.Y., 2021. A description of the advanced research WRF version 4. NCAR Tech. Note NCAR/TN-556+STR 145. https://doi.org/10.5065/1dfh-6p97.

Tao, C., Jiang, H., 2015. Distributions of shallow to very deep precipitation– convection in rapidly intensifying tropical cyclones. J. Clim. 28, 8791–8824.
Tao, W.K., Chen, J.P., Li, Z., Wang, C., Zhang, C., 2012. Impact of aerosols on convective clouds and precipitation. Rev. Geophys. 50.
Thompson, G., Eidhammer, T., 2014. A study of aerosol impacts on clouds and precipitation development in a large winter cyclone. J. Atmos. Sci. 71, 3636–3658.
Van Den Heever, S.C., Cotton, W.R., 2007. Urban aerosol impacts on downwind convective storms. J. Appl. Meteorol. Climatol. 46, 828–850.
Varble, A.C., Igel, A.L., Morrison, H., Grabowski, W.W., Lebo, Z.J., 2023. Opinion: a critical evaluation of the evidence for aerosol invigoration of deep convection. Atmos. Chem. Phys. 23, 13791–13808.
Wang, Y., Zhang, Z., Chow, W.S., Wang, Z., Yu, J.Z., Chi-Hung Fung, J., Shi, X., 2023. Investigating the effect of aerosol uncertainty on convective precipitation forecasting in South China's coastal area. J. Geophys. Res.-Atmos. 128 (10), e2023JD038694.
Wu, H., Peng, J., Liu, Y., Zhang, L., Li, Z., Zhang, W., 2024. On the local available energy budget of an idealized tropical cyclone. Atmos. Res. 310, 107655.
Yang, X., Zhou, L., Zhao, C., Yang, J., 2018. Impact of aerosols on tropical cyclone-induced precipitation over the mainland of China. Clim. Chang. 148, 173–185.
Yuan, T., Li, Z., Zhang, R., Fan, J., 2008. Increase of cloud droplet size with aerosol optical depth: an observation and modeling study. J. Geophys. Res. Atmos. 113.
Zhang, H., McFarquhar, G.M., Cotton, W.R., Deng, Y., 2009. Direct and indirect impacts of Saharan dust acting as cloud condensation nuclei on tropical cyclone eyewall development. Geophys. Res. Lett. 36.